

Influence of Magnetic Geometry on Scrape-off Layer Profiles

C. J. Boswell, J. L. Terry, B. LaBombard, B. Lipschultz

May 22, 2002

Abstract

Using a filtered and absolutely calibrated visible imaging camera tangentially viewing the inner wall of the Alcator C-Mod tokamak, it was observed that the D_α emission profile peaked at the secondary separatrix. A one-dimensional physical space, two-dimensional velocity kinetic neutral code [4] was used to simulate the neutrals in the region near the inner wall. The plasma profiles were required as inputs to the code and measured values from the low-field-side scrape-off layer were used by keeping the values constant on a magnetic flux surface. For the model to reproduce the observed measurements a sharp decay in the plasma density, with a scale length of *sim* 3mm, at the secondary separatrix was artificially introduced. The model and the observations were in good agreement and indicate the emission profile has two scale lengths, 1) on the high-field-side of the emission peak due to the plasma density profile and 2) on the low-field-side of the emission peak due to an effective ionization mean-free-path on neutrals originating at the secondary separatrix.

1 Introduction

Little work has been published on measuring or characterizing the scrape-off layer (SOL) near the inner wall of a diverted tokamak. Work that has been done has noted significant differences between the inner SOL (high-field-side) and the outer (low-field-side) SOL. On Alcator C (a limited tokamak) it was noted that there was a poloidal variation in density in shadow of the limiter with the minimum occurring on the high-field-side. [6] Another result was that the radial density e-folding length also had a minimum value on the high-field-side of the SOL, with the maximum occurring on the low-field-side of the SOL. Another interesting result is from the ASDEX tokamak (a diverted tokamak), where it was observed that fluctuations typical of the low-field-side SOL would be observed on the high-field-side SOL when in a single null discharge, but when in a balanced double null discharge the fluctuations were absent from the high-field-side SOL. [2] More recently, it has been observed on Alcator C-Mod that the D_α emission at the inner SOL peaks not on the primary separatrix, as is observed on the low-field-side SOL, but on the secondary separatrix. The previous, but not fully understood, observations along with the more recent observations from Alcator C-Mod has prompted a more thorough investigation into the inner SOL profiles.

2 Experimental Technique

On Alcator C-Mod [3] the D_α emission from the inner wall region was measured using a tangentially-viewing visible imaging CCD camera. [1] The camera was absolutely calibrated and filtered for D_α emission using an interference filter located directly in-front of the lens.

The camera is located 19.5 cm below the midplane of the tokamak and has a slight upward tilt of ~ 5 degrees. One dimensional emission profiles are generated from the horizontal viewing chords at 19.5 cm below the midplane. Figure 1 shows an image from the camera showing the viewing chords used to determine the emission profile, and figure 2 shows the poloidal projection of the camera view on a cross-section of the tokamak noting the view of the chords used in determining the emission profile.

The brightness profiles from the horizontal viewing chords was fit to the Abel integral of an emission profile having the form:

$$\epsilon(r) = \begin{cases} c_0 \exp\left[\frac{r-r_0}{\lambda_-}\right] & \text{if } r \leq r_- \\ \epsilon_0 + c_1 (r - r_0)^2 & \text{if } r_- \leq r \leq r_+ \\ c_2 \exp\left[\frac{-r+r_0}{\lambda_+}\right] & \text{if } r_+ \leq r \end{cases} , \quad (1)$$

where ϵ_0 is the peak emissivity of the profile, r_0 is the location of the center of the profile, λ_- is the high-field side (HFS) exponential scale length of the emission profile, λ_+ is the low-field side (LFS) exponential scale length of the emission profile, c_1 is a measure of the “peakedness” of the emission profile. By requiring that the emission profile be differentiable, all other constants can be found using the previously described variables. With these parameters the effect the magnetic geometry has on the D_α emission can be quantified.

3 Magnetic Geometry

In a balanced double null discharge there exist two distinct regions of the scrape-off layer, a high-field side scrape-off layer (inner scrape-off layer) and a low-field side scrape-off layer (outer scrape-off layer). In an unbalanced double null configuration these two regions still

exist outside the secondary separatrix. Between the primary and secondary separatrix there exists a region of the scrape-off layer in which the low- and high-field sides are magnetically connected (common scrape-off layer). Figure 2 shows the three regions (inner, outer, and common scrape-off layer) in a typical lower single null discharge.

To investigate the influence the magnetic geometry has on the D_α emission near the inner wall the magnetic configuration was scanned dynamically from a lower single null (LSN) to a double null (DN) through to an upper single null (USN). The global parameters for this experiment were typical of an L-mode discharge on Alcator C-Mod and kept nearly constant: $B_T = 5.4$ T, $I_p = 0.8$ MA, $\bar{n}_e \approx 10^{20}$ m⁻³. The main magnetic effect of this scan is the location of the secondary separatrix with respect to the primary separatrix, from ~ 1 cm from the primary separatrix at the outboard midplane to having no secondary separatrix during double null back to being ~ 1 cm from the primary separatrix with a change in the null with which the secondary separatrix is associated.

4 Observations

Fitting the brightness measurements as described in section 2 the variation of the location of the emissivity peak (r_0), the HFS emission scale length (λ_-), and the LFS emission scale length (λ_+) were observed. The location of the emissivity peak is summarized in figure 3, and can clearly be seen to follow the secondary separatrix regardless of the null with which the secondary separatrix is associated. The HFS emission scale length, shown in figure 4, is relatively constant within the error of this measurement. The LFS emission scale length has a smaller error associated with its measurement and has a reduction of the scale length when

the discharge is near double null configuration. The LFS emission scale length measurements are summarized in figure 5.

All three of these observations can be explained by a steep plasma density decay beginning at the secondary separatrix and decaying towards the inner wall and a relatively flat plasma density profile in the common SOL. In this case the neutral atoms would travel freely until they came near the secondary separatrix where they would begin to ionize. In the common SOL the neutrals would have a nearly constant ionization rate and their density would decay exponentially with a $1/e$ length approximately equal to the ionization mean-free-path. Since the D_α emissivity is a product of the neutral and electron densities and has a weak dependence on temperature in the temperature range expected ($T_e \geq 5$ eV), the HFS emission scale length would be indicative of the electron density scale length and the LFS emission scale length would be indicative of the ionization mean-free-path with the peak in the emission occurring at the secondary separatrix or where the product of the densities is a maximum.

5 Modeling

A one dimensional space, two dimensional velocity, kinetic neutral code (KN1D) [4] was used to simulate the plasma-neutral interactions near the inner wall of the tokamak. This code requires as inputs the plasma profiles (temperature, density, and velocity) and the neutral pressure at the inner wall. KN1D uses many molecular and atomic processes to determine the distribution functions of both the atomic and molecular neutrals. The processes included are (1) charge exchange collisions, (2) electron-impact ionization and dissociations, (3) elastic

self-collisions (atomic and molecular), and (4) a variety of elastic cross-collisions (atom-ion, atom-molecule, molecule-ion).

The inputs used in simulating the inner wall SOL region included using typical plasma profiles in the common SOL, as measured on the LFS midplane by a scanning Langmuir probe, and a sharp decay of the plasma density in the inner SOL ($\lambda_n = 3$ mm) beginning at the secondary separatrix. Using the LFS common SOL values for the plasma profile in the HFS common SOL is adequate since the LFS emission scale length in the KN1D output only changed by a few percent when the common SOL density profiles was varied from a flat density to a flat temperature profile while keeping pressure constant on a flux surface. The input value of the neutral pressure at the inner wall is unimportant since the absolute scale of the KN1D output D_α emissivity is a linear function of this neutral pressure. When the neutral pressure at the inner wall was chosen to agree with the measured emissivity profile the pressures required were in the range of 0.6 to 3 mTorr.

The results of the simulations show an excellent agreement with the location of the emission peak (figure 3) and the LFS emission scale length (figure 5) and only a moderate agreement with the HFS emission scale length (figure 4). The constancy of the HFS emission scale length is because the D_α emission profile on the HFS of the peak is dominated by the plasma density profile, which is given as an input to the code. Therefore the HFS emission scale length in the output of KN1D could be made to agree better with the measurement but, the value from KN1D is within the error of the measurement and to better match the model with the measured results would only use more computing time with no more physics understanding. The LFS emission scale length from KN1D agrees well with the measured

scale length and confirms that it is due to an average ionization mean-free-path since the scale length shortens as the secondary separatrix approaches the core or hotter denser plasma.

6 Conclusions

Summarizing the observed and simulated results, we note (1) the D_α emissivity peaks on the secondary separatrix, (2) the HFS emission scale length has no systematic dependence on the magnetic geometry, and (3) the LFS emission scale length decreases as the discharge approaches a double null configuration. The location of the emission and the independence of the HFS emission scale length can be explained by a sharp plasma density decay beginning at the secondary separatrix and decreasing toward the inner wall. The HFS emission scale length is a measure of the plasma density decay length. The LFS emission scale length can be explained by the ionization mean-free-path of the neutrals into the common SOL, and therefore is a measure of the effective ionization mean-free-path for the neutrals originating at the secondary separatrix.

The location and sharp decay of the plasma density beginning at the secondary separatrix can be explained by considering the typical SOL paradigm. In the SOL paradigm all plasma in the SOL flows along field lines to the divertor plate and the radial plasma profiles are determined by this parallel transport. On the LFS of the common SOL and in the outer SOL it is believed that there is strong radial transport flattening the plasma profiles contrary to the typical SOL paradigm. [7], [5] On the HFS we believe the profiles in the common SOL are set by the LFS dynamics and that in the inner SOL the profiles are more in line with the SOL paradigm. This explanation is consistent with the previous observations mentioned

in section 1. The density decay length is shorter at the HFS of Alcator C because it was not connected to the LFS. The fluctuations measured at the inner wall on ASDEX during single-null discharges is the effect of the LFS dynamics on the HFS common SOL, while the lack of measured fluctuations during double-null discharges occur because the inner SOL is again not connected to the LFS and therefore does not experience its effects.

References

- [1] C. J. Boswell, J. L. Terry, B. Lipschultz, and J. Stillerman. Applications of visible ccd cameras on the alcator c-mod tokamak. *Review of Scientific Instruments*, 72(1):935–9, Jan 2001.
- [2] M. Endler, H. Niedermeyer, L. Giannone, E. Holzhauser, A. Rudyj, G. Theimer, N. Tsois, and ASDEX Team. Measurements and modelling of electrostatic fluctuations in the scrape-off layer of asdex. *Nuclear Fusion*, 35(11):1307–1339, 1995.
- [3] I. H. Hutchinson, R. Boivin, F. Bombarda, P. Bonoli, S. Fairfax, C. Fiore, J. Goetz, S. Golovato, R. Granetz, M. Greenwald, S. Horne, A. Hubbard, J. Irby, B. LaBombard, B. Lipschultz, E. Marmor, G. McCracken, M. Porkolab, J. Rice, J. Snipes, Y. Takase, J. Terry, S. Wolfe, C. Christensen, D. Garnier, M. Graf, T. Hsu, T. Luke, M. May, A. Niemczewski, G. Tinios, J. Schacter, and J. Urbahn. First results from alcator c-mod. *Physics of Plasmas*, 1(5):1511–1518, May 1994.
- [4] B. LaBombard. Kn1d: A 1-d space, 2-d velocity, kinetic transport algorithm for atomic and molecular hydrogen in an ionizing plasma. PSFC-RR-01-3.

- [5] B. LaBombard, R. L. Boivin, M. Greenwald, J. Hughes, B. Lipschultz, D. Mossessian, C. S. Pitcher, J. L. Terry, and S. J. Zweben. Particle transport in the scrape-off layer and its relationship to discharge density limit in alcator c-mod. *Physics of Plasmas*, 8(5):2107–17, May 2001.
- [6] B. LaBombard and B. Lipschultz. Poloidal asymmetries in the scrape-off layer plasma of the alcator c tokamak. *Nuclear Fusion*, 27(1):81–99, 1987.
- [7] B. LaBombard, M. V. Umansky, R. L. Boivin, J. A. Goetz, J. Hughes, B. Lipschultz, D. Mossessian, C. S. Pitcher, and J. L. Terry. Cross-field plasma transport and main-chamber recycling in diverted plasmas on alcator c-mod. *Nuclear Fusion*, 40(12):2041–60, Dec 2000.

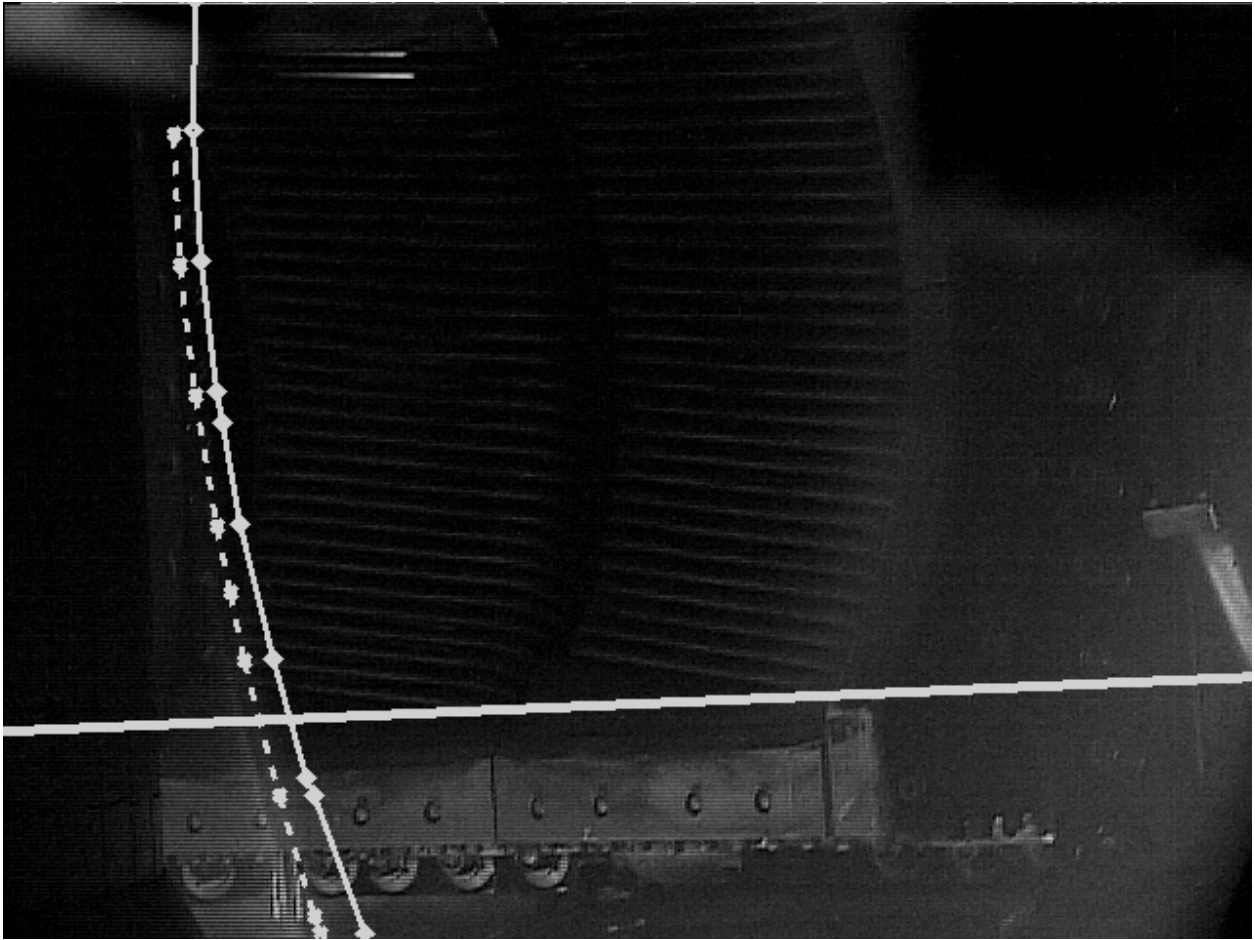


Figure 1: An image from that camera showing the inner wall, the primary separatrix, the secondary separatrix, and the horizontal chords used in generating the emission profile.

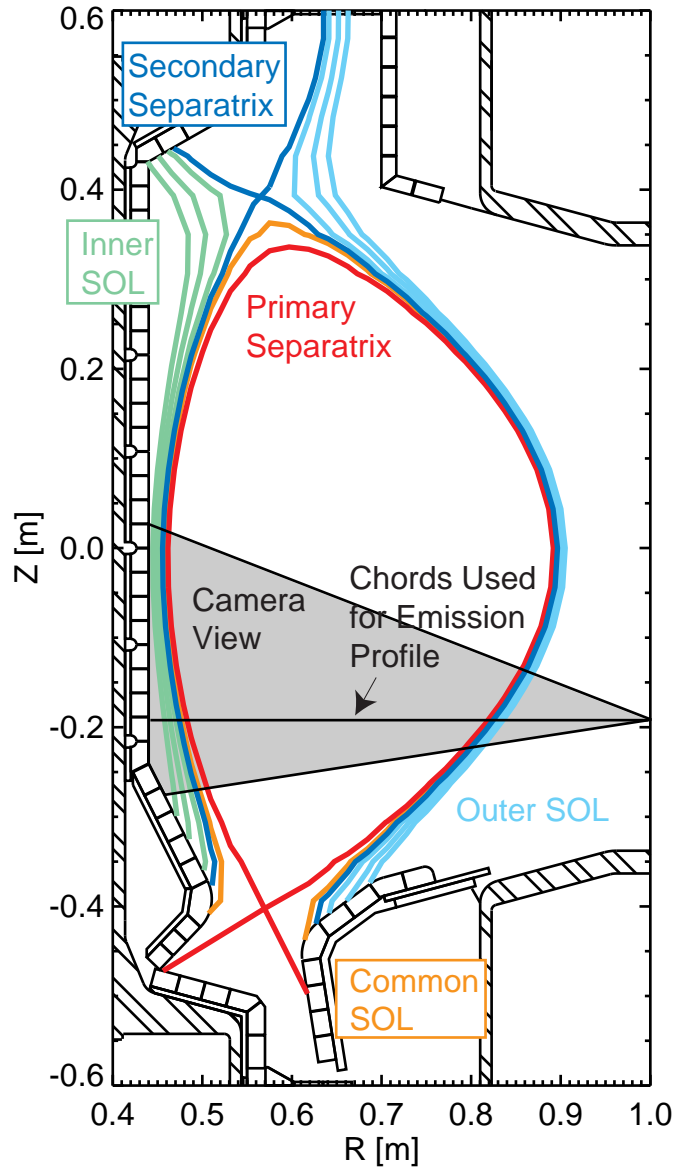


Figure 2: The inner, outer and common scrape-off layer in a typical lower single null discharge, along with the poloidal projection of the camera view.

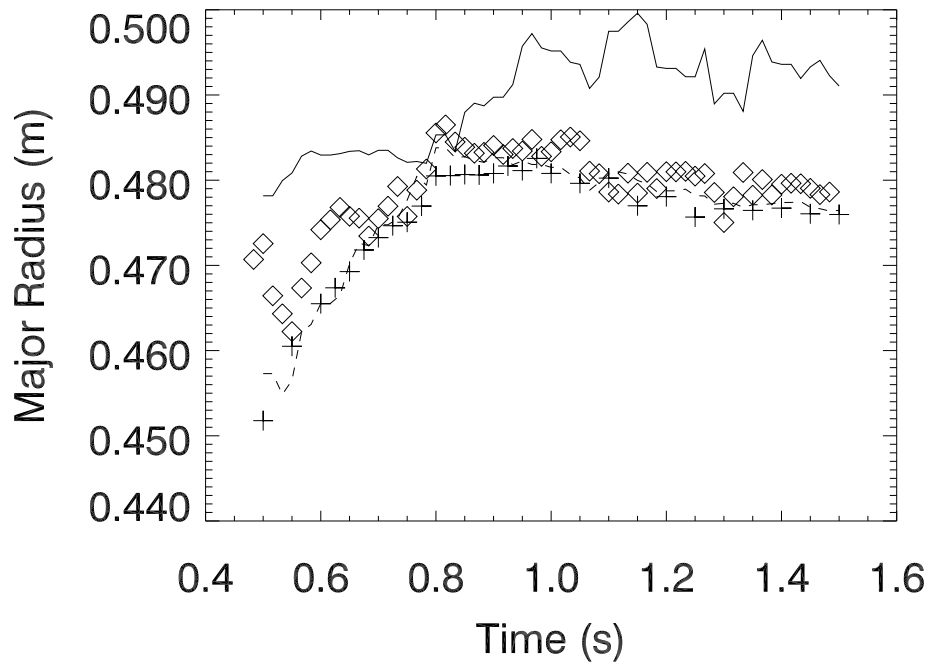


Figure 3: Plot showing the location of the peak in the emission from the observations (\diamond) and the location of the peak in the emission from the kinetic neutral code KN1D (+) with respect to the location of the primary (—) and secondary (---) separatrices.

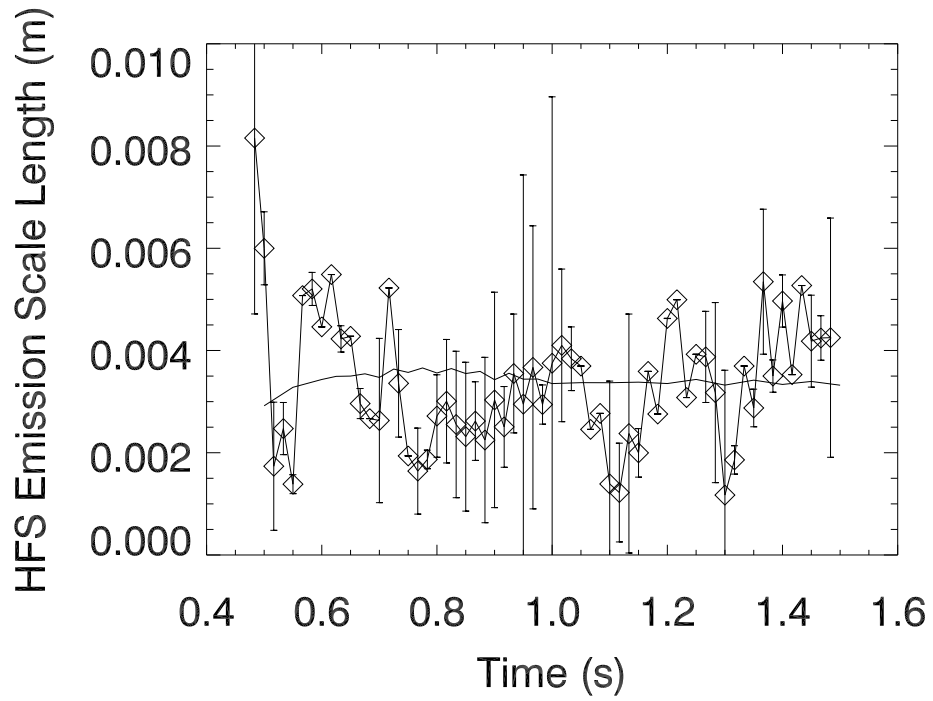


Figure 4: Plot showing the high-field-side emission scale length measured from the observations (\diamond) and the high-field-side emission scale length calculated from the kinetic neutral code KN1D (-).

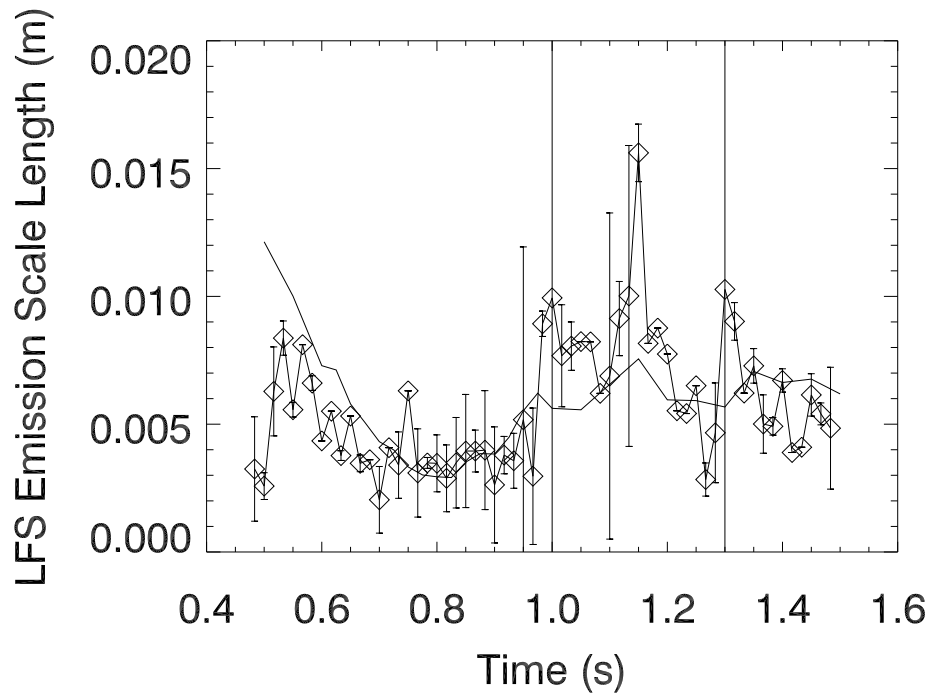


Figure 5: Plot showing the low-field-side emission scale length measured from the observations (\diamond) and the low-field-side emission scale length calculated from the kinetic neutral code KN1D (-).